

# ROUGHENING OF ION-ERODED SURFACES

A.-L. BARABÁSI, M. A. MAKEEV, C. S. LEE

*Department of Physics, University of Notre Dame, Notre Dame, IN 46556*

R. CUERNO

*Departamento de Matemáticas and Grupo Interdisciplinar de Sistemas Complicados,  
Universidad Carlos III de Madrid, c/ Butarque 15, 28911 Leganés, SPAIN*

Recent experimental studies focusing on the morphological properties of surfaces eroded by ion-bombardment report the observation of self-affine fractal surfaces, while others provide evidence about the development of a periodic ripple structure. To explain these discrepancies we derive a stochastic growth equation that describes the evolution of surfaces eroded by ion bombardment. The coefficients appearing in the equation can be calculated explicitly in terms of the physical parameters characterizing the sputtering process. Exploring the connection between the ion-sputtering problem and the Kardar-Parisi-Zhang and Kuramoto-Sivashinsky equations, we find that morphological transitions may take place when experimental parameters, such as the angle of incidence of the incoming ions or their average penetration depth, are varied. Furthermore, the discussed methods allow us to calculate analytically the ion-induced surface diffusion coefficient, that can be compared with experiments. Finally, we use numerical simulations of a one dimensional sputtering model to investigate certain aspects of the ripple formation and roughening.

## 1 Introduction

In the last decade we have witnessed the development of an array of theoretical tools, ideas and techniques intended to describe and characterize the growth and roughening of nonequilibrium surfaces<sup>1,2,3,4</sup>. Initiated by advances in understanding the statistical mechanics of various nonequilibrium systems, it has been observed that for most surfaces in nature the roughness follows simple scaling laws. These surfaces are self-affine fractals, being characterized by the roughness or self-affine exponent  $\alpha$ . One of the main advantage of this description is that various growth processes can be classified into universality classes that share the same scaling exponents. On the practical side this means that the scaling exponents characterizing roughness do not vary continuously, but are defined by the universality class to which they belong.

One particularly important thin film processing technique is ion beam sputtering<sup>5,6,7</sup>. Sputtering is the removal of material from the surface of solids through the impact of energetic particles. It is a widespread technique, used in a large number of applications, with a remarkable level of sophistication. It is a basic tool in surface analysis, depth profiling, sputter cleaning, microma-

chining, and sputter deposition.

Motivated by the advances in understanding growth, and by the need of having a detailed knowledge on the morphology of the sputter eroded surfaces, recently a number of experimental studies have investigated the morphological properties of surfaces eroded by ion bombardment. Briefly, the experimental results can be classified in two main classes. There exists ample evidence about the development of a periodic ripple structure in sputter etched surfaces<sup>8,9,10,11,12,13</sup>. However, a number of recent investigations have provided rather detailed and convincing experimental evidence, that under certain experimental conditions ion-eroded surfaces are rough and self-affine, and the roughness follows the predictions of various scaling theories<sup>14,15,16</sup>. Moreover, these investigations did not find evidence of ripple formation on the surface!

The discrepancy between the results of the mentioned investigations motivated us to have a second look at the mechanisms shaping the morphology of ion eroded surfaces<sup>17</sup>. In this paper we investigate the large scale properties of ion-sputtered surfaces aiming to understand in an unified framework the various dynamic and scaling behaviors of the experimentally observed surfaces. For this we derive a stochastic nonlinear equation that describes the time evolution of the surface height. The coefficients appearing in the equation are functions of the physical parameters characterizing the sputtering process. We find that transitions may take place between various surface morphologies as the experimental parameters (e.g. angle of incidence, penetration depth) are varied. Namely, at short length-scales the equation describes the development of a periodic ripple structure, while at larger length-scales the surface morphology may be either logarithmically ( $\alpha = 0$ ) or algebraically ( $\alpha > 0$ ) rough. Furthermore, we calculate analytically the ion-induced diffusion constant,  $D^I$ , and its dependence on the ion energy, flux, angle of incidence, and penetration depth. We find that there exists a parameter range when ion bombardment generates a *negative* surface diffusion constant, leading to morphological instabilities along the surface, affecting the surface roughness and the ripple structure. The effect of ion-induced diffusion on the morphology of ion-sputtered surfaces is summarized in a morphological phase diagram, allowing for direct experimental verification of our predictions. Finally, we use numerical simulations of a one dimensional sputtering model to investigate certain aspects of the ripple formation and roughening.

## 2 Scaling theory

A common feature of most non-equilibrium rough interfaces<sup>1,2,3</sup> observed experimentally or in discrete models is that their roughening follows simple scal-

ing laws. The associated scaling exponents can be obtained using numerical simulations or stochastic evolution equations. The morphology and dynamics of a two-dimensional rough surface can be characterized with the *interface width*, defined by the rms fluctuation in the height variable  $h(x, y, t)$ ,

$$W(L, t) \equiv \sqrt{\frac{1}{L^2} \langle \sum_{x, y=1, L} [h(x, y, t) - \bar{h}]^2 \rangle}, \quad (1)$$

where  $L$  is the linear size of the sample, the brackets  $\langle \dots \rangle$  denote ensemble average, and the *mean height* of the surface,  $\bar{h}$ , is defined by

$$\overline{h(t)} \equiv \frac{1}{L^2} \sum_{x, y=1, L} h(x, y, t). \quad (2)$$

For times  $t \gg t_\times \sim L^z$ , the surface width behaves as

$$W(L, t) \sim L^\alpha, \quad (3)$$

where  $\alpha$  is the *roughness exponent* and  $z$  is the *dynamic exponent*. Regarding the early dynamics of the roughening process, the total width increases as  $W(L, t) \sim t^\beta$ , where  $\beta$  is the *growth exponent*. The dynamic exponent is related to  $\alpha$  and  $\beta$  as  $z = \alpha/\beta$ <sup>18</sup>.

To understand the roughening process, we need to develop methods to predict the value of the scaling exponents  $\alpha$  and  $\beta$ . A breakthrough in this direction was the introduction of the Kardar-Parisi-Zhang (KPZ) equation<sup>19</sup>

$$\frac{\partial h}{\partial t} = \nu \nabla^2 h + \lambda (\nabla h)^2 + \eta(x, y, t) \quad [KPZ]. \quad (4)$$

The first term on the rhs describes the relaxation of the interface due to the surface tension  $\nu$  and the second is a generic nonlinear term incorporating lateral growth. The noise,  $\eta(x, y, t)$ , reflects the random fluctuations in the growth process and is an uncorrelated random number that has zero configurational average. For one dimensional interfaces the scaling exponents of the KPZ equation are known exactly, as  $\alpha = 1/2$ ,  $\beta = 1/3$ , and  $z = 3/2$ . However, for higher dimensions they are known only from numerical simulations. For the physically most relevant two dimensional interface we have  $\alpha \simeq 0.38$  and  $\beta \simeq 0.18$ <sup>20</sup>.

If  $\lambda = 0$  in (4), the remaining equation describes the equilibrium fluctuations of an interface which tries to minimize its area. This equation, introduced and studied in the context of interface roughening by Edwards and Wilkinson (EW)<sup>21</sup>, can be solved exactly due to its linear character, giving the scaling exponents  $\alpha = (2-d)/2$  and  $\beta = (2-d)/4$ . For two dimensional interfaces we have  $\alpha = \beta = 0$ , leading to a logarithmic roughening of the interface.

### 3 Experimental results

The morphology of surfaces bombarded by energetic ions has long fascinated the experimental community. Lately, with the development of high resolution observation techniques, this question is living a new life.

We shall focus here on two dominant morphologies, ripple formation and kinetic roughening, since these are observed in the sputtering of impurity free, amorphous materials. Impurities that bind strongly to the surface (being thus difficult to sputter) may induce other dominant morphological features, such as cones or abrupt walls<sup>8</sup>. These will not be considered in this paper. Also, we limit ourselves to sputtering by ion bombardment, in which the ions have parallel trajectories and the same velocity. Thus we will not consider plasma etching (where the ions have a broad energy distribution and random angles of incidence) or chemical sputtering, where the yield is influenced by the chemical reactions taking place on the surface.

#### 3.1 Ripple formation

Ripple formation on ion-sputtered surfaces have been observed by many groups in various systems and ion beams (for a review see<sup>8</sup>). Here we discuss a few recent investigations that characterized in great detail the observed morphologies.

Evidence for the ripple structure on the surfaces of SiO<sub>2</sub> and Ge has been provided in a series of studies by Chason *et al.*<sup>9,10,11,12</sup>. We shall discuss here the results obtained on SiO<sub>2</sub><sup>10,11</sup>. A low energy ion beam (Xe, H or He), with energies  $\leq 1$  keV is directed towards a SiO<sub>2</sub> sample with an angle of incidence of 55° from normal. The typical incoming flux is  $10^{13}$  cm<sup>-2</sup>s<sup>-1</sup>. The interfaces are analyzed using *in situ* energy dispersive x-ray reflectivity and *ex situ* atomic force microscopy (AFM). Bombarding the surface with 1 keV Xe ions, one finds that the interface roughness, determined from X-ray diffraction, increases linearly with the fluence (the fluence is the number of incoming atoms per surface area, and plays the role of time in these measurements). Thus  $\beta = 1$ , too large a value to be interpretable by continuum theories. Such a large value of  $\beta$  indicates the existence of an instability in the system. Physically, the instability is balanced by surface diffusion, leading to the appearance of the ripple structure whose wavelength increases with temperature. Such a ripple structure can be seen if one inspects the AFM pictures of the interface. A similar ripple structure has been observed for Ge surfaces bombarded by Xe atoms<sup>9</sup>.

Another series of experiments on ripple formation were reported by MacLaren *et al.*<sup>13</sup>. They studied InP and GaAs bombardment with 5 keV Ar<sup>+</sup>,

17 keV  $\text{Cs}^+$  and 5.5 keV  $\text{O}_2^+$  beams in a temperature range of  $-50$  to  $200$   $^\circ\text{C}$ . Their study revealed in detail the temperature dependence of the ripple wavelength. For example for GaAs bombarded by  $\text{Cs}^+$  ions the ripple spacing increased from zero  $0.89\text{ }\mu\text{m}$  to  $2.0\text{ }\mu\text{m}$ , as the temperature increased from  $0$   $^\circ\text{C}$  to  $100$   $^\circ\text{C}$ . Probably the most interesting finding of their study was that when lowering the temperature, the ripple spacing (wavelength) did not go continuously to zero, as one would expect, since the diffusion constant decreases exponentially with the inverse temperature, but rather at around  $20$   $^\circ\text{C}$  it stabilized at an approximately constant value. MacLaren *et al.* interpreted this as the emergence of a radiation enhanced diffusion, that gives a constant (temperature independent) contribution to the diffusion constant. We shall return to ion enhanced diffusion in Sects. 6. and 7.

### 3.2 Roughening

For graphite bombarded with 5 keV Ar ions, Eklund *et al.*<sup>14</sup> reported  $\alpha \simeq 0.2 - 0.4$ , and  $z \simeq 1.6 - 1.8$ , values consistent with the predictions of the Kardar-Parisi-Zhang (KPZ) equation in 2+1 dimensions<sup>19,20</sup>. No trace was found of a periodic ripple structure. In these experiments pyrolytic graphite was bombarded by 5 keV Ar ions, which arrived with an angle of incidence of  $60^\circ$ . The experiments were carried out for two flux values,  $6.9 \times 10^{13}$  and  $3.5 \times 10^{14}$  ions/ $\text{cm}^2$ , and the total fluences obtained were  $10^{16}$ ,  $10^{17}$  and  $10^{18}$ . The etched graphite was examined using STM. Large scale features develop with continuous bombardment, the interface becoming highly correlated and rough.

A somewhat larger roughness exponent has been measured for samples of iron bombarded with 5 keV Ar arriving with angle of incidence of  $25^\circ$ . The interface morphology was observed using STM, and the height-height correlation function results in a roughness exponent  $\alpha = 0.53 \pm 0.02$ <sup>15</sup>. The mechanism leading to such a roughness exponent is not yet understood in terms of the continuum theories, since for two dimensions the growth equations predict 0.38,  $2/3$  and 1, all values far from the observed value.

Finally Si(111) sputtered by 0.5 keV  $\text{Ar}^+$  ions has also been observed to roughen, in this case following an anomalous dynamic scaling form  $w(t, \ell) \sim \ln(t)\ell^{2\alpha}$ , with  $\alpha \simeq 1.15 \pm 0.08$ <sup>16</sup>, where  $w(t, \ell)$  is the surface width for a small window of lateral size  $\ell$ .

## 4 Continuum theory

#### 4.1 Sigmund's theory of sputtering

In order to calculate the sputtering yield, and predict the surface morphology, we first need to understand the mechanism of sputtering, resulting from the interaction of the incident ion and the surface layer.

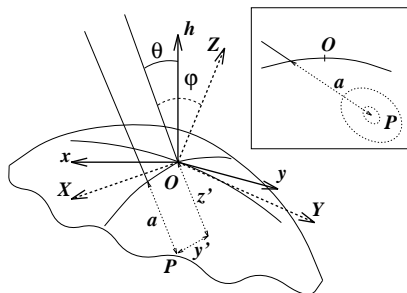


Figure 1: Reference frames for the computation of the erosion velocity at point  $O$ . Inset: Following a straight trajectory (solid line) the ion penetrates an average distance  $a$  inside the solid (dotted line) after which it completely spreads out its kinetic energy. The dotted curves are equal energy contours. Energy released at point  $P$  contributes to erosion at  $O$ .

A qualitative picture is as follows<sup>8</sup> (see Fig. 1). The incoming ions penetrate the surface and transfer their kinetic energy to the atoms of the substrate by colliding with the substrate atoms, or through other processes such as electronic excitations. Atoms that recoil with sufficient energy undergo secondary collisions, thereby generating another generation of recoiling atoms. A vast majority of atoms will not gain enough energy to leave their lattice position permanently. However, some are permanently removed from their sites, locally making the substrate amorphous. The atoms that are near the surface and gain enough energy to break their bonds and leave the surface will be sputtered. The scattering events that might lead to sputtering take place within a certain layer of average depth  $a$ . Usually the number of sputtered atoms is orders of magnitudes smaller than the total number of atoms participating in the collision cascade.

A rather successful theory of the above processes was introduced by Sigmund to describe the experimentally observed sputtering yields<sup>22</sup>. His treatment considers the energy transfer from the incoming ion to the atoms of an isotropic solid by writing down a Boltzmann transport equation for the atoms. Expanding this equation in form of Legendre polynomials, he obtains a solution using the method of moments. One of the most important result of his analysis is that for low energies the damage and energy distribution generated by the incoming ion follows a Gaussian. Thus here, following<sup>22,23</sup>, we consider

that the average energy deposited at point  $O$  due to the ion arriving at  $P$  follows the Gaussian distribution

$$E(\mathbf{r}') = \frac{\epsilon}{(2\pi)^{3/2}\sigma\mu^2} \exp\left\{-\frac{z'^2}{2\sigma^2} - \frac{x'^2 + y'^2}{2\mu^2}\right\}. \quad (5)$$

In (5)  $z'$  is the distance measured along the ion trajectory, and  $x'$ ,  $y'$  are measured in the plane perpendicular to it (see Fig. 1; for simplicity in the figure  $x'$  has been set to 0);  $\epsilon$  denotes the total energy carried by the ion and  $\sigma$  and  $\mu$  are the widths of the distribution in directions parallel and perpendicular to the incoming beam, respectively. However, the sample is subject to a uniform flux  $J$  of bombarding ions. A large number of ions penetrate the solid at different points simultaneously and the velocity of erosion at  $O$  depends on the total power  $\mathcal{E}_O$  contributed by all the ions deposited within the range of the distribution (5). If we ignore shadowing effects among neighboring points, as well as further redeposition of the eroded material, the normal velocity of erosion at  $O$  is given by

$$v = p \int_{\mathcal{R}} d\mathbf{r} \Phi(\mathbf{r}) E(\mathbf{r}), \quad (6)$$

where the integral is taken over the region  $\mathcal{R}$  of all the points at which the deposited energy contributes to  $\mathcal{E}_O$ ,  $\Phi(\mathbf{r})$  is a local correction to the uniform flux  $J$  and  $p$  is a proportionality constant between power deposition and rate of erosion. In the following we review the basic steps in the calculation of  $v$ ; further details can be found in Refs.<sup>17,24,23</sup>.

#### 4.2 Continuum equation for the surface height

In this section we derive an equation of motion for the surface height from the physical model of ion-sputter erosion discussed in the previous section. Since we are mainly interested in the physically relevant case of a two dimensional substrate and the one dimensional case to linear order is very clearly explained in the work by Bradley and Harper<sup>23</sup>, we refer the reader to that reference, and focus here on the more general 2d case.

In the following we summarize the steps in the derivation of the equation of motion.

(i) First we calculate the normal component of the velocity of erosion  $v_O$  at a generic point  $O$  of the interface. This calculation is most easily performed in a local frame of reference  $(X, Y, Z)$  defined as follows: the  $\hat{Z}$  axis is identified with the normal direction to the average surface orientation at  $O$ . Moreover  $\hat{Z}$  forms a plane with the trajectory of an ion penetrating the surface at  $O$ . We

choose the  $\hat{X}$  axis to lie in that plane. Finally,  $\hat{Y}$  is the remaining direction which completes a right-handed reference frame, see Fig. 1.

(ii) Next we relate the quantities measured in coordinates of the local frame to coordinates in the laboratory frame  $(x, y, h)$ . The latter is defined by the experimental configuration. That is,  $h$  is the direction normal to the uneroded flat surface. The ion trajectories together with the  $h$  axis define a plane, which is taken to be the  $x-h$  plane. And finally the  $y$  axis completes a right-handed reference frame, see Fig. 1. However,  $\varphi$ , which is the angle between the ion trajectory and the *local* normal to the surface, changes from point to point along the surface, and is a function of the local values of the slopes at  $O$  (as seen in the laboratory frame), as well as of the fixed angle  $\theta$  subtended by the ion trajectories and the normal to the uneroded surface (the  $h$  direction in Fig. 1).

(iii) In the absence of overhangs the surface can be described by a single valued height function  $h(x, y, t)$ , measured from an initial flat configuration which is taken to lie in the  $(x, y)$  plane. The ion beam is parallel to the  $x-h$  plane forming an angle  $0 \leq \theta < \pi/2$  with the  $z$  axis. To obtain the equation of motion for the surface profile function  $h(x, y, t)$ , we will have to project the normal component of the velocity of erosion onto the global  $h$  axis. We get

$$\frac{\partial h(x, y, t)}{\partial t} \simeq -v(\varphi, R_X, R_Y) \sqrt{1 + (\nabla h)^2}, \quad (7)$$

where  $\varphi$  is the angle of the beam direction with the local normal to the surface at  $h(x, y, t)$  and  $R_{X,Y}$  the values of the local radii of curvature at  $(x, y, h)$ . Now  $\varphi$  is a function of the angle of incidence  $\theta$  and the values of the local slopes  $\partial_x h$  and  $\partial_y h$ , and can be expanded in powers of the latter. We will assume that the surface varies smoothly enough so that products of derivatives of  $h$  can be neglected for third or higher orders.

At this stage additional relevant physical processes must be taken into account to describe the evolution of the surface. First, the bombarding ions reach the surface at random positions and times. We account for the stochastic arrival of ions by adding to (7) a Gaussian white noise  $\eta(x, y, t)$  with zero mean and variance proportional to the flux  $J$ . Second, at finite temperature atoms diffuse on the surface<sup>9,14</sup>. To include this surface self-diffusion we allow for a term  $-D_T \nabla^2 (\nabla^2 h)$ <sup>25,26</sup>, where  $D_T$  is a temperature dependent positive coefficient. Expanding (7) and adding the noise and the surface-diffusion terms we obtain the equation of motion<sup>27</sup>

$$\frac{\partial h}{\partial t} = -v_0 + \gamma \frac{\partial h}{\partial x} + \nu_x \frac{\partial^2 h}{\partial x^2} + \nu_y \frac{\partial^2 h}{\partial y^2} + \frac{\lambda_x}{2} \left( \frac{\partial h}{\partial x} \right)^2 + \frac{\lambda_y}{2} \left( \frac{\partial h}{\partial y} \right)^2$$



$$-D_x^I \frac{\partial^4 h}{\partial x^4} - D_y^I \frac{\partial^4 h}{\partial y^4} - D_T \nabla^2 (\nabla^2 h) + \eta. \quad (8)$$

From (7) we can compute the expressions for the coefficients appearing in (8) in terms of the physical parameters characterizing the sputtering process. To simplify the discussion we restrict ourselves to the symmetric case  $\sigma = \mu$ . The general case is discussed in<sup>17</sup>. If we write  $F \equiv (\epsilon J p / \sqrt{2\pi}) \exp(-a_\sigma^2/2 - a_\sigma^2 s^2)$ ,  $s \equiv \sin \theta$ ,  $c \equiv \cos \theta$  and  $a_\sigma \equiv a/\sigma$ , we find for the coefficients in (8)

$$\begin{aligned} v_0 &= \frac{F}{\sigma} c, \quad \gamma = \frac{F}{\sigma} s (a_\sigma^2 c^2 - 1), \\ \lambda_x &= \frac{F}{\sigma} c \{ a_\sigma^2 (3s^2 - c^2) - a_\sigma^4 s^2 c^2 \}, \\ \lambda_y &= -\frac{F}{\sigma} c \{ a_\sigma^2 c^2 \}, \\ \nu_x &= \frac{F}{2} a_\sigma \{ 2s^2 - c^2 - a_\sigma^2 s^2 c^2 \}, \\ \nu_y &= -\frac{F}{2} a_\sigma c^2, \\ D_x^I &= \frac{F a^2}{24 a_\sigma} \{ a_\sigma^4 s^4 c^2 + a_\sigma^2 (6c^2 s^2 - 4s^4) + 3c^2 - 12s^2 \}, \\ D_y^I &= \frac{F a^2}{24 a_\sigma} 3c^2. \end{aligned} \quad (9)$$

## 5 Analysis of the obtained growth equations

Consistent with the direction of the bombarding beam and the choice of coordinates, the terms in (8) are symmetric under  $y \rightarrow -y$  but not under  $x \rightarrow -x$ , while for  $\theta \rightarrow 0$  we get  $\gamma = \xi_x = \xi_y = 0$ ,  $\lambda_x = \lambda_y$  and  $\nu_x = \nu_y$ . The equation studied in Ref.<sup>23</sup> corresponds to the deterministic linear version of (8), i. e.  $\lambda_x = \lambda_y = \eta = 0$ .

If  $\nu_x$  and  $\nu_y$  are positive, the surface diffusion term is expected to contribute negligibly to the relevant surface relaxation mechanism when we probe the system at increasingly large length scales. Scaling properties are then described by the anisotropic KPZ equation (AKPZ), which predicts two possible behaviors depending on the relative signs of the coefficients  $\lambda_x$  and  $\lambda_y$ <sup>28,29</sup>. If  $\lambda_x \lambda_y > 0$ , then  $\alpha = 0.38$  and  $z = 1.6$ , the surface width  $W(L, t)$  increases algebraically, being characterized by the exponents of the KPZ equation in 2+1 dimensions<sup>20</sup>. For  $\lambda_x \lambda_y < 0$ , the nonlinear terms  $\lambda_x$  and  $\lambda_y$  become irrelevant, and the width grows only logarithmically, i.e.  $\alpha = 0$ .

In our case  $\nu_x$  can change sign as  $\theta$  and  $a_\sigma$  are varied, while  $\nu_y$  is always negative. The negative  $\nu$  causes an instability, whose origin is the faster erosion for the bottom of a trough than for the peak of a crest, as predicted by (6)<sup>22,23</sup> (see also Fig. 3 of Ref. <sup>23</sup>). An instability due to a negative surface tension is also known to take place in the Kuramoto–Sivashinsky (KS) equation<sup>30</sup>, which is the *noiseless* and isotropic version of (8). It has been argued for the KS equation that in 1+1 dimensions  $\nu$  renormalizes to a positive value<sup>31</sup>, and the large length scale behavior is described by the KPZ equation. In 2+1 dimensions it is not completely settled whether the large distance behaviors of KS and KPZ fall in the same universality class, different approaches leading to conflicting results<sup>32</sup>.

In contrast to the KS equation, Eq. (8) is anisotropic, and explicitly contains a noise term. The competition between surface tension and surface diffusion generates a characteristic length scale in the system,  $\ell_c = \sqrt{D_T/|\nu|}$ , where  $\nu$  is the largest in absolute value of the negative surface tension coefficients. Below we discuss a possible scenario for the scaling behavior predicted by (8) based primarily on the results available in the literature for some of its limits. The complete scaling picture should be provided by either a DRG analysis capable of coping with the linear instabilities present in the system, or a numerical integration of (8).

The scaling behavior depends on the relative signs of  $\nu_x$ ,  $\nu_y$ ,  $\lambda_x$  and  $\lambda_y$ <sup>33</sup>. The variations of these coefficients as functions of  $a_\sigma$  and  $\theta$  lead to the phase diagram shown in Fig. 2.

*Regions I and II*— For small  $\theta$  both  $\nu_x$  and  $\nu_y$  are negative. As discussed by Bradley and Harper<sup>23</sup> and experimentally studied by Chason *et al.*<sup>9</sup>, a periodic structure dominates the surface morphology, with ripples oriented along the direction ( $x$  or  $y$ ) which presents the largest absolute value for its surface tension coefficient. The observed wavelength of the ripples is  $\lambda_c = 2\pi\sqrt{2}\ell_c$ .

The large length scale behavior  $\ell \gg \ell_c$  is expected to be different. Now both nonlinearities and the noise may become relevant. The scaling properties of the surface morphologies predicted by (8) are unknown. A possible scenario is that the  $\nu$ 's renormalize to positive values, as they do for the KS equation in 1 + 1 dimensions, and the large scale scaling properties of the system are described by the AKPZ equation. Then one would observe algebraic scaling in region *I*, where both nonlinearities have the same (negative) sign, whereas scaling would become logarithmic through an AKPZ-like mechanism in region *II*, where  $\lambda_x$  and  $\lambda_y$  have opposite signs. Actually, the asymptotic KPZ scaling has been recently shown to occur along the  $\theta$  axis of Fig. 2 through a renormalization group analysis<sup>34</sup>.

*Region III* — This region is characterized by a positive  $\nu_x$  and a negative

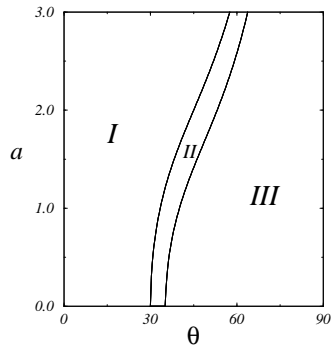


Figure 2: Phase diagram for the isotropic case  $\sigma = \mu = 1$ . Region I:  $\nu_x < 0$ ,  $\nu_y < 0$ ,  $\lambda_x < 0$ ,  $\lambda_y < 0$ ; Region II:  $\nu_x < 0$ ,  $\nu_y < 0$ ,  $\lambda_x > 0$ ,  $\lambda_y < 0$ ; Region III:  $\nu_x > 0$ ,  $\nu_y < 0$ ,  $\lambda_x > 0$ ,  $\lambda_y < 0$ . Here  $a$  is measured in arbitrary units and  $\theta$  is measured in degrees.

$\nu_y$ . Now the periodic structure associated with the instability is directed along the  $y$  direction and is the dominant morphology at scales  $\ell \sim \ell_c$ . Again, such an anisotropic and linearly unstable equation is unexplored in the context of growth equations. Assuming that  $\nu_y$  renormalizes to a positive value, and that the AKPZ mechanism operates, one would expect logarithmic scaling in region *III*, since the nonlinear terms have opposite signs.

Even though several aspects of the scaling behavior predicted by (8) and (9) remain to be clarified, we believe that these equations contain the relevant ingredients for understanding roughening by ion bombardment<sup>35</sup>. To summarize, at short length scales the morphology consists of a periodic structure oriented along the direction determined by the largest in absolute value of the negative surface tension coefficients<sup>9</sup>. Modifying the values of  $a_\sigma$  or  $\theta$  changes the orientation of the ripples<sup>8,23</sup>. At large length scales we expect two different scaling regimes. One is characterized by the KPZ exponents, which *might* be observed in region *I* in Fig. 2. Indeed, the values of the exponents reported by Eklund *et al.*<sup>14</sup> are consistent within the experimental errors with the KPZ exponents in 2+1 dimensions. The other regions (*II* and *III*) are characterized by logarithmic scaling ( $\alpha = 0$ ), which has not been observed experimentally so far. Moreover, by tuning the values of  $\theta$  and/or  $a_\sigma$  one may induce transitions among the different scaling behaviors. For example, fixing  $a_\sigma$  and increasing the value of  $\theta$  would lead from KPZ scaling (region *I*) to logarithmic scaling (*II*, *III*) for large enough angles.

Recent results by Rost and Krug on the two dimensional anisotropic KS equation indicate that the scaling regimes *II* and *III* in the *noiseless* limit of our model is dominated by exponentially growing solutions of the KS equation

<sup>36</sup>. In those regions the ripple structure is oriented along a direction which is neither  $x$  nor  $y$ . Further numerical simulations are needed to understand the effect of the noise on the stability of the exponential solutions. Insight into the expected morphologies is obtained from numerical simulation of discrete models, correctly capturing the basic mechanisms taking place during sputtering. Recent simulations on discrete models indicate that the noisy KS equation indeed describes the dynamics of the sputtering generated roughening <sup>37</sup>.

## 6 Ion-Induced Surface Diffusion in Ion Sputtering

In the absence of ion bombardment surface diffusion is thermally activated, and characterized by the diffusion constant,  $D_T = D_0 \exp[-E_d/k_B T]$ , such that the evolution of the surface height,  $h(x, y, t)$  is described by the continuum equation  $\partial h / \partial t = -D_T \nabla^4 h$  <sup>25</sup>. Here  $E_d$  is the activation energy for surface diffusion of the adatoms and  $T$  is the substrate temperature. However, numerous experiments regarding the effect of ion bombardment on island formation, surface migration, surface smoothing and ripple formation have provided evidence that ion bombardment is accompanied by an increase in surface diffusion <sup>13,39,40,41,42,43</sup>. In particular, it has been demonstrated that ion-induced surface diffusion can decrease the epitaxial temperature <sup>39</sup>, enhance nucleation during growth <sup>40</sup>, modify the surface morphology, or induce the existence of a temperature independent ion-induced surface diffusion constant, as in the experiments of MacLaren *et al.* referred to above.

Although the effect of the ions on surface diffusion is well documented experimentally, there is no theory that would quantify it. Eq. (9) provides analytically the ion-induced diffusion constant,  $D^I$ , and its dependence on the ion energy, flux, angle of incidence, and penetration depth. Consistent with symmetry considerations for  $\theta = 0$  we obtain  $D_x^I = D_y^I$ . However, for  $\theta \neq 0$  we find that  $D_x^I \neq D_y^I$ , i.e. the ion-induced surface diffusion is *anisotropic*. Moreover, its sign also depends on the experimental parameters. Their properties can be summarized as follows: (a) Independent of the angle of incidence  $D_y^I$  is positive, and decreases with  $\theta$ , while the sign of the  $D_x^I$  depends on both  $\theta$  and  $a_\sigma$  as shown in Fig. 3. Thus, while for  $\theta = 0$  the ion bombardment enhances the surface diffusion ( $D_x^I > 0$ ), for large  $\theta$  it can suppress diffusion; (b) The fact that  $D_x^I$  can be negative indicates that any simple theory connecting the magnitude of the ion-induced diffusion to the energy transferred by the ions to the surface is incomplete, since it can predict only a positive  $D^I$ . In fact,  $D^I$  is the result of a complex interplay between the local *surface topography* and the energy transferred to the surface; (c) The diffusion constants are proportional to the flux  $J$ , in agreement with the detailed exper-

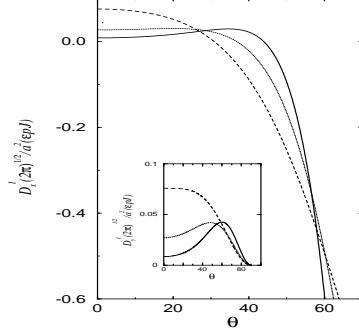


Figure 3: Ion-induced diffusion constant,  $D_x^I$  and  $D_y^I$  (inset) as a function of the angle of incidence  $\theta$ . In both figures the curves correspond to  $a_\sigma = 1.5$  (dashed line),  $a_\sigma = 2.0$  (dotted line) and  $a_\sigma = 2.5$  (continuous line).

imental study of Cavaille and Dreschner<sup>42</sup>; (d) It is a standard experimental practice to report the magnitude of the ion-enhanced diffusion using an effective temperature  $T^{eff}$  at which the substrate needs to be heated to obtain the same mobility as with ion bombardment<sup>42,43</sup>. We can calculate  $T^{eff}$  using the relation  $D^I + D_0 \exp(-E_a/k_B T) = D_0 \exp(-E_a/k_B T^{eff})$ , that has two important consequences. First, the anisotropic diffusion constant translates into an anisotropic  $T^{eff}$ , i.e. we have  $T_x^{eff} \neq T_y^{eff}$ . The experimental methods used to estimate  $T^{eff}$  could not distinguish  $T_x^{eff}$  and  $T_y^{eff}$ <sup>42,43</sup>. However, current observational methods should be able to detect the difference between the two directions. Second, while it is generally believed that ion bombardment can only raise the effective temperature since it transfers energy to the surface, the negative  $D^I$  indicates that along the  $x$  direction one could have  $T_{eff} < T$ . (e) Finally, the results (9) are based on Sigmund's theory of sputtering<sup>22</sup>, that describes sputtering in the linear cascade regime. The energy range when this approach is applicable lies between 0.5 keV and 1 MeV, the precise lower and upper limits being material dependent. Thus, we do not expect (9) to apply to low energy (few eV) ion-enhanced epitaxy.

*Quantitative comparison with experiments*— At nonzero temperature the total diffusion constant is given by  $D = D^I + D_T$ . As  $T$  decreases there is a critical temperature,  $T_c$ , at which  $D^I = D_T$ , so that for  $T < T_c$  the diffusion is dominated by its ion-induced component, which is independent of temperature, in agreement with the experimental results of MacLaren *et al.*

<sup>13</sup>. Unfortunately, for most materials the quantities entering in  $F$ ,  $a_\sigma$  and  $D_0$  are either unknown, or only their order of magnitude can be estimated. However, we can express  $T_c$  in terms of measurable quantities independent of these constants

$$T_c = \frac{T_0}{1 - (2T_0 k_B / E_a) \ln(\ell_{Ion} / \ell_{T_0})} \quad (10)$$

where  $\ell_{T_0}$  is the experimentally measured ripple wavelength at any temperature  $T_0 > T_c$ ;  $\ell_{Ion}$  is the ripple wavelength in the low temperature regime,  $T < T_c$ , where ion induced diffusion dominates, and therefore  $\ell_{Ion}$  is independent of  $T$ ;  $E_a$  is provided by the slope of  $\ln(\ell)$  versus  $1/T$  in the high temperature regime ( $T \gg T_c$ ). Consequently, *all* quantities in (10) can be obtained from a plot of the ripple wavelength as a function of temperature, so (10) gives  $T_c$  *in terms of measurable quantities*. Such a plot is provided by MacLaren *et al.*<sup>13</sup>, leading to  $E_a = 0.51\text{eV}$ ,  $\ell_{Ion} = 0.8\mu\text{m}$ . Using  $\ell_{T_0} = 2\mu\text{m}$  for  $T = 368\text{K}$ , we obtain  $T_c = 57^\circ\text{C}$ , which is in good agreement with the experiments, that provide  $T_c$  between  $45$  and  $60^\circ\text{C}$ <sup>13</sup>.

*Morphological phase diagram*— The detailed morphological phase diagram is rather complex if the diffusion is not thermally activated, but ion-induced. At low temperatures, when  $D_T$  is negligible, the ripple wavelengths are  $\ell_x^I = 2\pi\sqrt{D_x^I/|\nu_x|}$  and  $\ell_y^I = 2\pi\sqrt{D_y^I/|\nu_y|}$ . In the following we discuss the expected surface morphologies in function of the experimental parameters  $\theta$  and  $a_\sigma$ , based on the phase diagram shown in Fig. 4.

*Region I*— The surface tensions,  $\nu_x$  and  $\nu_y$ , are negative, while  $D_x$  and  $D_y$  are positive, consequently we have a superimposed ripple structure along the  $x$  and the  $y$  directions. The ripple wavelength observed experimentally is the smallest of the two, and since  $\ell_x^I > \ell_y^I$  the ripple wave vector is oriented along the  $y$  direction. The lower boundary of this region separating it from Region II is given by the solution of the  $\ell_x^I = \ell_y^I$  equation.

*Region II*— Here the ripple wave vector is oriented along the  $x$  direction, since  $\ell_x^I < \ell_y^I$ . This region is bounded below by the  $D_x^I = 0$  line. At large length scales in I and II one expects kinetic roughening described by the KPZ equation<sup>1,2,17,19,44</sup>.

*Region III* — In this region  $D_x^I$  is negative, while the sign of all other coefficients are as in I and II. Since both the surface tension and the surface diffusion are destabilizing along  $x$ , every mode is unstable and one expects that the KPZ nonlinearity cannot turn on the KS stabilization<sup>17,34</sup>, the system being unstable at large length scales as well, leading to exponential growth. The lower boundary of this region is given by the  $\nu_x = 0$  line.

*Region IV* — Here we have  $\nu_x > 0$ ,  $\nu_y < 0$ ,  $D_x^I < 0$  and  $D_y^I > 0$ , i.e. one expects the surface to be periodically modulated in the  $y$  direction. In the  $x$

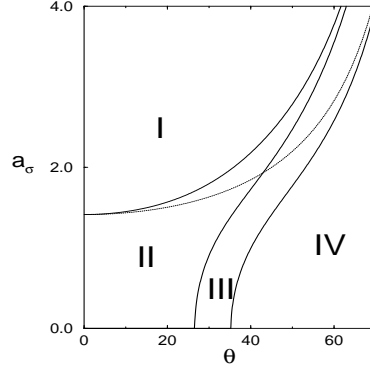


Figure 4: Phase diagram for the isotropic case  $\sigma = \mu = 1$  at  $T < T_c$ . Region I:  $\nu_x < 0$ ,  $\nu_y < 0$ ,  $D_x^I > 0$ ,  $D_y^I > 0$  and  $\ell_x > \ell_y$ ; Region II:  $\nu_x < 0$ ,  $\nu_y < 0$ ,  $D_x^I > 0$ ,  $D_y^I > 0$ , and  $\ell_x < \ell_y$ ; Region III:  $\nu_x < 0$ ,  $\nu_y < 0$ ,  $D_x^I < 0$  and  $D_y^I > 0$ ; Region IV:  $\nu_x > 0$ ,  $\nu_y < 0$ ,  $D_x^I < 0$  and  $D_y^I > 0$ . Note that the phase diagram is independent of the precise values of  $J$  and  $p$ , while the  $\epsilon$  dependence is contained in  $a_\sigma$ .

direction we have an interesting reversal of the instability: the short length scale instability generated by the negative  $D_x^I$  is stabilized by the positive surface tension  $\nu_x$ . Thus there is no ripple structure along the  $x$  direction. Regarding the large length scale behavior, along the  $x$  direction the surface diffusion term is irrelevant compared to the surface tension, thus one expects KPZ scaling. However, along the  $y$  direction the KS mechanism is expected to act, renormalizing the negative  $\nu_y$  to positive values for length scales larger than  $\ell_y^I$ , leading to a large wavelength KPZ behavior.

If thermal and ion-induced diffusion coexist, the ripple wavelengths are given by  $\ell_x = 2\pi[(D_T + D_x^I)/|\nu_x|]^{1/2}$  and  $\ell_y = 2\pi[(D_T + D_y^I)/|\nu_y|]^{1/2}$ . The phase diagram for intermediate temperatures can be calculated using the total  $D$ . In particular for high  $T$ , when  $D_T \gg D_x^I$  and  $D_T \gg D_y^I$ , the phase diagram converges to the one obtained in Ref. <sup>17</sup>, the ripple orientation being controlled by the  $\nu_x = \nu_y$  line (dotted line in Fig. 3). Thus with increasing  $D_T$  the phase boundary between the regions I and II converges to the  $\nu_x = \nu_y$  line and the  $D_x = 0$  boundary separating the regions II and III shifts downwards, eventually disappearing. However, in the intermediate regions new phases with coarsening ripple domains <sup>36</sup> appear as the  $D_x^I = 0$  line crosses the  $\nu_x = 0$  line.

While we limited our discussion to the effect of the ion-induced diffusion on the surface morphology, the results (9) can be used to investigate other

phenomena as well, such as island nucleation. The experimental verification of the above results would constitute an important step to elucidate the mechanism responsible for ion-induced diffusion, with potential applications to ion-enhanced epitaxy as well.

## 7 Atomistic models

The methods employed for the modeling of growth phenomena at the atomic level range from first-principle calculations, to molecular dynamics, and Monte Carlo (MC) simulations<sup>45</sup>. However, currently only MC methods can reach the long time scales and fairly large length scales needed to observe ripple formation and roughening. Moreover, the general features of ripple formation and roughening are rather generic, suggesting the existence of a *material independent robust mechanism* governing them. Thus simple models that incorporate the basic physics of the system, i.e. ion-bombardment and surface diffusion, should be successful in capturing the observed behavior, see *e.g.* Ref.<sup>37</sup>. We have developed atomistic MC models of erosion that include ion-bombardment, ion-induced atom removal and activated surface diffusion. To model *surface diffusion* we use the methods developed for MBE, taking the diffusion rate of an atom proportional to  $\exp[-E_a/k_B T]$ , where  $E_a$  is the activation energy for diffusion and  $T$  is temperature<sup>1</sup>.

To model the ion-bombardment we assume that the ion beam has a constant flux, but the time and the position when and where an ion strikes the surface is random. The ion penetrates the bulk reaching a penetrating depth  $a$  and releases its kinetic energy (see inset of Fig. 1). The energy reaching the surface atoms,  $E_{ion}$ , is calculated using the energy distribution (5). If  $E_{ion}$  is larger than the desorption energy  $\tilde{E}_d = nE_B + E_0 + E_d$ , where  $n$  is the number of nearest neighbors, then it will be sputtered. If  $E_{ion}$  is smaller than  $\tilde{E}_d$ , then it will contribute either to surface diffusion with probability  $\exp[-(nE_B + E_0 - E_{ion})/k_B T]$  or to breaking the bonds (sputtering) with probability  $\exp[-(\tilde{E}_d - E_{ion})/k_B T]$ . In the simulation we used  $\epsilon=1000$  eV,  $\sigma=\mu=a=10.9$  lattice constants,  $E_0 = 0.4$  eV,  $E_B = 0.1$  eV, and  $E_d=1.0$  eV.

We used the structure factor,  $S(k) \equiv \langle h(k, t)h(-k, t) \rangle$ , where  $h(k, t)$  is the Fourier transform of  $h(x, t)$ , to estimate the ripple wavelength  $\ell$ . Typically  $S(k)$  develops a sharp maximum, which allows us to estimate  $\ell$ . However, at large erosion times the structure factor reflects the roughening of the substrate as well, thus the maximum will slowly disappear. Similarly, the maximum is more visible at low temperatures than at large  $T$ .

Fig. 5 shows the ripple wavelength as a function of temperature for  $\theta = 0$ . At large temperatures  $\ell$  follows an Arrhenius law, however, at low  $T$  it con-



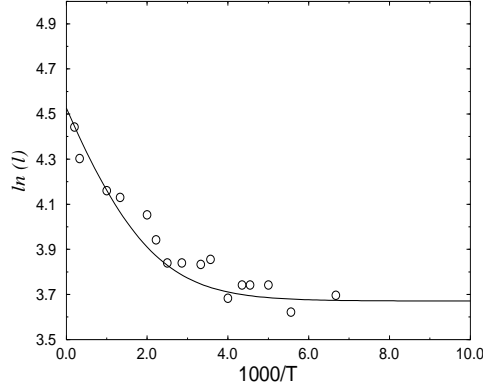


Figure 5: Ripple wavelength as a function of the inverse temperature obtained in the numerical simulations of a one dimensional sputtering model. The continuous line represents an analytical fit (see the text).

verges to a constant value. These results are reminiscent of the experimental data of Maclaren *et al.*<sup>13</sup>, providing direct numerical evidence of ion enhanced surface diffusion. Indeed, using  $\ell = 2\pi\sqrt{D_T + D^I}$ , where  $D_T$  follows an Arrhenius law  $D_T = D_0 \exp(-E_a/kBT)$ , we can obtain an excellent fit to the data in Fig. 5. Furthermore, the fit also allows us to determine the diffusion coefficients in our simulation, providing  $D_0 = 7000$ ,  $E_a = 0.08\text{eV}$ , and  $D^I = 1543$ . There are two observations we have to make analyzing these results. First,  $E_a$  is much lower than the activation energy we used as an input to the simulations. However, this is not in contradiction: the effective activation energy felt by the diffusing atoms is lowered by the energy provided by the ions. This effect lowers  $E_a$ . Indeed, we measured the average activation energy  $E_a^{eff} = E_a - E_i$  for the atoms, the result agreeing in order of magnitude with the  $E_a^{eff}$  obtained from the fit in Fig. 5. Second,  $D_0$  is smaller than the experimentally expected values, that are of order  $10^{xx}$ , but agrees with the smaller diffusive activity we can obtain in the numerical simulations (due to running time limitations). It is easy to see that a larger  $D_0$  would lead to a more extended high-temperature region, such as the one observed by MacLaren *et al.*<sup>13</sup>.

## 8 Acknowledgment

We would like to acknowledge discussions and comments by L. A. N. Amaral, G. Grinstein, K. B. Lauritsen, H. Makse, L. M. Sander, and H. E. Stanley. This research was partially supported by the University of Notre Dame Faculty Research Program.

## 9 References

1. A.-L. Barabási and H. E. Stanley, *Fractal Concepts in Surface Growth* (Cambridge University Press, Cambridge, 1995).
2. *Dynamics of Fractal Surfaces*, F. Family and T. Vicsek, eds. (World Scientific, Singapore, 1991).
3. P. Meakin, Phys. Rep. **235**, 189 (1993); T. Halpin-Healey and Y.-C. Zhang, Phys. Rep. **254**, 215 (1995); W.M. Tong, and R.S. Williams, Annu. Rev. Phys. Chem. **45**, 401 (1994).
4. J. Krug and H. Spohn, in *Solids Far From Equilibrium: Growth, Morphology and Defects*, edited by C. Godrèche (Cambridge Univ. Press, Cambridge, England, 1991);
5. *Sputtering by Particle Bombardment*, R. Behrisch, ed. (Springer-Verlag, Heidelberg 1981, 1983), Vols. I, II, III.
6. *Handbook of Ion Beam Processing Technology*, J.J. Cuomo, S.M. Rossnagel, and H.R. Kaufman, eds. (Noyes Publications, Park Ridge 1992).
7. *Ion Beam Assisted Film Growth*, T. Itoh ed. (Elsevier, Amsterdam, 1989).
8. G. Carter, B. Navinšek and J. L. Whitton in Vol. II of Ref. <sup>5</sup>, p. 231.
9. E. Chason *et al.*, Phys. Rev. Lett. **72**, 3040 (1994).
10. T. M. Mayer, E. Chason and A. J. Howard, J. Appl. Phys. **76**, 1633 (1994).
11. E. Chason, T. M. Mayer, and A. Payne, Appl. Phys. Lett. **60**, 2353 (1992).
12. E. Chason and T. Mayer, Appl. Phys. Lett. **62**, 363 (1993).
13. S.W. MacLaren, J.E. Baker, N.L. Finnegan, and C.M. Loxton, J. Vac. Sci. Technol. A **10**, 468 (1992).
14. E. A. Eklund, *et al.*, Phys. Rev. Lett. **67**, 1759 (1991); E. A. Eklund, E. J. Snyder and R. S. Williams, Surf. Sci. **285**, 157 (1993).
15. J. Krim *et al.*, Phys. Rev. Lett. **70**, 57 (1993).
16. H.-N. Yang, G.-C. Wang, and T.-M. Lu, Phys. Rev. **B 50**, 7635 (1994).
17. R. Cuerno and A.-L. Barabási, Phys. Rev. Lett. **74**, 4746 (1995); A.-L. Barabási and R. Cuerno, [Proc. MRS Fall Meeting, Vol. 407, Boston

- 1995] (MRS, Pittsburgh, 1995).
18. F. Family and T. Vicsek, J. Phys. A **18**, L75 (1985).
  19. M. Kardar, G. Parisi and Y.-C. Zhang, Phys. Rev. Lett. **56**, 889 (1986).
  20. J. M. Kim and J. M. Kosterlitz, Phys. Rev. Lett. **62**, 2289 (1989); B. M. Forrest and L. Tang, J. Stat. Phys. **60**, 181 (1990); J.G. Amar and F. Family, Phys. Rev. A **41**, 3399 (1990); K. Moser, D. E. Wolf and J. Kertész, Physica A **178**, 215 (1991); T. Ala Nissila *et al.*, J. Stat. Phys. **72**, 207 (1993).
  21. S. F. Edwards and D. R. Wilkinson, Proc. R. Soc. London A **381**, 17 (1982).
  22. P. Sigmund, Phys. Rev. **184**, 383 (1969); J. Mat. Sci. **8**, 1545 (1973).
  23. R. M. Bradley and J. M. E. Harper, J. Vac. Sci. Technol. A **6**, 2390 (1988).
  24. R. Cuerno and A.-L. Barabási, (unpublished).
  25. C. Herring, J. Appl. Phys. **21**, 301 (1950); W. W. Mullins, J. Appl. Phys. **28**, 333 (1957); in the context of stochastic models see D. E. Wolf and J. Villain, Europhys. Lett. **13**, 389 (1990); S. Das Sarma and P. I. Tamborenea, Phys. Rev. Lett. **66**, 325 (1991).
  26. J. Villain, J. Phys. I **1**, 19 (1991).
  27. In the expansion of (7) two additional nonlinearities are obtained on the rhs of Eqn. (8):  $\xi_x \frac{\partial h}{\partial x} \frac{\partial^2 h}{\partial x^2} + \xi_y \frac{\partial h}{\partial x} \frac{\partial^2 h}{\partial y^2}$ , where  $\xi_x$  and  $\xi_y$  are functions of  $a$ ,  $\sigma$ ,  $\mu$  and  $\theta$ <sup>24</sup>. One can see that  $\xi_x$  and  $\xi_y$  are irrelevant at large length scales using the known values of  $\alpha$  and  $z$ <sup>20</sup> for both the nonlinear and the linear fixed points in 2+1 dimensions.
  28. D. E. Wolf, Phys. Rev. Lett. **67**, 1783 (1991).
  29. The relevance of the AKPZ equation to sputter erosion has been suggested by R. Bruinsma in *Surface Disordering: Growth, Roughening and Phase Transitions*, R. Jullien *et al.* eds. (Nova Science, New York, 1992).
  30. Y. Kuramoto and T. Tsuzuki, Prog. Theor. Phys. **55**, 356 (1977); G. I. Sivashinsky, Acta Astronaut. **6**, 569 (1979).
  31. S. Zaleski, Physica D **34**, 427 (1989); K. Sneppen *et al.* Phys. Rev. A **46**, 7352 (1992); F. Hayot, C. Jayaprakash, and Ch. Josserand, Phys. Rev. E **47**, 911 (1993); V. S. L'vov *et al.*, Nonlinearity **6**, 25 (1993).
  32. I. Procaccia *et al.* Phys. Rev. A **46**, 3220 (1992); V. S. L'vov and I. Procaccia, Phys. Rev. Lett. **69**, 3543 (1992); *ibid.* **72**, 307 (1994); C. Jayaprakash, F. Hayot, and R. Pandit, Phys. Rev. Lett. **71**, 12 (1993); *ibid.* **72**, 308 (1994).
  33. The terms  $-v_0$  and  $\partial_x h$  can be reabsorbed by a change of variables to a comoving frame, and do not affect the scaling properties.
  34. R. Cuerno, and K.B. Lauritsen, Phys. Rev E **52**, 4853 (1995).

35. Our analysis describes the roughening process in the small slope approximation. However, at late stages additional non-linear effects, such as shadowing may become relevant [For a review see G. S. Bales *et al.*, Science **249**, 264 (1990).]
36. M. Rost, and J. Krug, Phys. Rev. Lett. **75**, 3894 (1995).
37. R. Cuerno, H.A. Makse, S. Tomassone, S.T. Harrington, and H.E. Stanley, Phys. Rev. Lett. **75**, 4464 (1995); K.B. Lauritsen, R. Cuerno, and H.A. Makse, Phys. Rev E **54**, 3577 (1996).
38. A.-L. Barabási and M. Makeev (to be published).
39. V.O. Babaev, Ju.V. Bukov, and M.B. Guseva, Thin Solid Films **38**, 1 (1976).
40. M. Marinov, Thin Solid Films **46**, 267 (1977).
41. S.A. Barnett, H.F. Winters, and J.E. Greene, Surf. Sci. **181**, Zh.I. Dranova and I.M. Mikhailovskii, Soviet Physics-Solid State **12**, 104 (1970); E. Chason *at al.*, Appl. Phys. Lett. **57**, 1793 (1990); E. Kay and S. M. Rossnagel, in *Handbook of Ion Beam Processing Technology*, in Ref. <sup>5</sup>. (1987).
42. J.Y. Cavaille and M. Drechsler, Surf. Sci. **75**, 342 (1978).
43. S.M. Rossnagel, R.S. Robinson, and H.R. Kaufman, Surf. Sci. **123**, 89 (1982).
44. W.M. Tong, and R.S. Williams, Annu. Rev. Phys. Chem. **45**, 405 (1994); J. Kertész and T. Vicsek, in *Fractals in Science*, edited by A. Bunde and S. Havlin (Springer-Verlag, Heidelberg, 1994).
45. E. Kaxiras, *Proceedings of the Workshop on Virtual Molecular Beam Epitaxy*, Ed. M.F. Gyure and J.J. Zinck, Comp. Mat. Sci. **6**, 113 (1996).